

# Intermodel and method comparison of mean radiant temperature from numerical weather prediction models: Evaluation of enhanced spatial resolution in Europe

Oleh SKRYNYK<sup>1,2,\*</sup> , Pavol NEJEDLÍK<sup>2</sup> ,  
Krzysztof BŁAŻEJCZYK<sup>3</sup> 

<sup>1</sup> Faculty of Geography and Regional Studies, University of Warsaw, Warsaw, Poland;  
e-mail: oleh.skrynyk@gmail.com

<sup>2</sup> Earth Science Institute, Slovak Academy of Sciences, Bratislava, Slovak Republic;  
e-mail: nejedlik@yahoo.com

<sup>3</sup> Institute of Geography and Spatial Organisation, Polish Academy of Sciences,  
Warsaw, Poland; e-mail: krzysztof@blazejczyk.eu

**Abstract:** Thermal stress indices play a vital role in evaluating human health risks related to heat and cold. Mean Radiant Temperature (MRT), derivable from numerical weather prediction (NWP) models, is a critical input for many such indices. This research generates high-resolution (5.5 km × 5.5 km) MRT estimates across Europe using the CERRA NWP system. We evaluate different computational approaches, benchmark the high-resolution MRT against the established ERA5-HEAT dataset, and validate results using BSRN ground observations. The study focuses on diverse European environments. Our high-resolution MRT product demonstrates comparable performance to ERA5-HEAT over flat terrain but offers substantial accuracy gains over complex terrain, including mountainous and coastal regions. These findings highlight the value of enhanced spatial resolution for accurate MRT estimation, crucial for robust thermal stress assessment and contributing to improved environmental health and safety strategies.

**Key words:** thermal stress, MRT, NWP, CERRA, ERA5, ERA5-HEAT, Europe, high-resolution

## 1. Introduction

Mean radiant temperature (MRT) is a key variable in human biometeorology, influencing thermal comfort and stress (*Höppe, 1999; McGregor, 2012*). Accurate MRT estimations are essential for various applications, including public health assessments, urban planning, and climate change impact studies (*Krüger, 2021*). Accurate estimations of Mean Radiant Temperature

---

\*corresponding author, e-mail: oleh.skrynyk@gmail.com

(MRT) become increasingly important for understanding and mitigating the impacts of thermal stress on human populations due to the rise of global temperatures and urbanisation. Inaccurate MRT estimations can result in assessments of thermal comfort, potentially impacting building design, urban planning, and public health interventions.

Traditionally, MRT has been estimated using in-situ measurements from instruments like globe thermometers or pyrgeometers (*ISO 7726:1998, 1998; Thorsson et al., 2007; VDI, 2008*). These methods often have limited spatial coverage and may be affected by local environmental factors (*Błażejczyk and Kunert, 2011*). More recently, remote sensing techniques have been employed to estimate MRT, utilising satellite data to derive thermal stress indices (*Wang et al., 2020*). While remote sensing offers broader spatial coverage, it can be limited by temporal resolution and atmospheric interference (*Voogt and Oke, 2003*). Empirical models have also been developed based on relationships between MRT and readily available meteorological variables, such as air temperature and radiation parameters (*Gál and Kántor, 2020*). These models provide simplicity and computational efficiency; however, they may not fully capture the complexity of MRT variations, particularly in urban environments (*Lindner-Cendrowska and Baranowski, 2023; Vanos et al., 2021*).

Numerical Weather Prediction (NWP) models have become valuable tools for estimating MRT. They offer advantages over traditional measurement methods by providing data that is spatially continuous and temporally dynamic (*Di Napoli et al., 2020b*). The growing availability of high-resolution NWP data can greatly enhance the accuracy of MRT estimations. This is especially important for regions with diverse topography and complex urban areas. The ERA5-HEAT dataset, derived from the ERA5 reanalysis, is commonly utilised for estimating mean radiant temperature (MRT). However, its spatial resolution of approximately 31 km by 31 km may restrict its capacity to capture detailed variations in MRT, particularly in regions with complex terrain or distinct microclimates (*Di Napoli et al., 2021*).

This study explores the potential of the Copernicus European Regional ReAnalysis (CERRA) to enhance MRT quantification (*Ridal et al., 2024*). The study aims to assess and compare the computation of MRT using CERRA system outputs, contrasting it with the established ERA5-HEAT

dataset. Furthermore, it aims to examine different methodologies utilised in calculating MRT components. Specifically, the investigation focuses on two distinct approaches: firstly, integrating the cosine of solar zenith angle over forecast steps using Gauss–Legendre quadrature versus employing sunlit-average; and secondly, comparing the direct component of solar downward radiation obtained from Numerical Weather Prediction models against computed values. The effectiveness of these combinations is evaluated through validation against station data sourced from the Baseline Surface Radiation Network. The analyses are based on case studies from January and July 2017. This study contributes to advancing our understanding of MRT computations (from intermodel and methodological differences) and emphasises the potential advantages of utilising enhanced spatial resolution in such analyses.

## 2. Data and methods

### 2.1. Copernicus European Regional ReAnalysis (CERRA)

The enhanced spatial resolution MRT was computed using radiation outputs from the CERRA NWP systems, which are part of the Copernicus Climate Change Service (C3S) and accessed from the Climate Data Store (CDS) (*Schimanke et al., 2021*). CERRA, developed as part of the Uncertainties in Ensembles of Regional Reanalyses (UERRA) project (<http://www.uerra.eu/>), aims to improve regional climate reanalysis for Europe and northern Africa. It consists of two components: the HARMONIE-ALADIN system and the MESCAN-SURFEX system. The HARMONIE-ALADIN system, with a horizontal resolution of 5.5 km and 106 vertical levels, uses 3-dimensional Variational Data Assimilation and incorporates boundary conditions from the ECMWF global reanalysis v5 (ERA5) (*Hersbach et al., 2020*). The MESCAN-SURFEX system, with a spatial resolution of 5.5 km, employs 2-dimensional Variational Data Assimilation to improve surface analyses (*Soci et al., 2016; Bazile et al., 2017*). These systems offer a comprehensive approach to regional climate reanalysis, integrating both atmospheric and surface dynamics.

CERRA variables are available as both analysis and forecast products (*Ridal et al., 2024; Schimanke et al., 2021*). The reanalysis is available with 3-hour timesteps. CERRA radiation data are accumulated fluxes over fore-

cast timesteps since the last analysis, and the values were resampled using subtractions of 1, 2, and 3 lead time hour forecasts to achieve 1-hour timesteps accumulations. The reanalysis is accessible with temporal coverage from September 1984 to the present (currently June 2021). Thus, the time step is set to 1 hour, and the spatial resolution is  $5.5 \text{ km} \times 5.5 \text{ km}$ .

## 2.2. Methodology for MRT calculation

MRT from NWP models could be computed using five long-wave and shortwave radiation fluxes at the surface: thermal downward radiation ( $L_{\text{surf}}^{\text{dn}}$ ) and its upwelling counterpart ( $L_{\text{surf}}^{\text{up}}$ ); direct ( $S_{\text{surf}}^{\text{dn,direct}}$ ) and diffuse ( $S_{\text{surf}}^{\text{dn,diffuse}}$ ) solar downward radiation and its upwelling counterpart ( $S_{\text{surf}}^{\text{up}}$ ). In the CERRA system, the upwelling components are absent and could be computed by subtracting the net radiations from downwards assuming the radiation budget equals 0. The same applies for diffuse solar downward radiation, which could also be computed from downwards by subtracting the total sky direct component; see *Hogan (2015)* for more details. The accumulated fluxes were divided by the accumulation period to convert into radiation means ( $\text{Wm}^{-2}$ ).

The methodology recently applied in ERA5-HEAT for MRT calculations was followed (*Di Napoli et al., 2020b*). The cosine of solar zenith angle ( $\text{cossza}$ ) is the crucial variable in the MRT regression function. The simplest way to calculate is to use the instantaneous formula:

$$\mu_0 = \sin \delta \sin \phi + \cos \delta \cos \phi \cos h, \quad (1)$$

from solar declination angle ( $\delta$ ), latitude ( $\phi$ ) and the hour angle in the local solar time ( $h = T + \lambda + \pi$ ), where  $T$  is the solar time in radians and  $\lambda$  is longitude (*Hogan and Hirahara, 2015, 2016*).  $\mu_0$  is clipped to 0 when the sun is below the horizon.

The instantaneous  $\text{cossza}$  with the accumulated radiation variables from NWPs overestimates MRT when  $\text{cossza}$  is close to 0, i.e. when the accumulation time includes sunrise or sunset hours (*Di Napoli et al., 2020b*). This happens because radiation in NWPs are usually accumulated fluxes over time ( $\text{Jm}^{-2}$ ), thus  $\text{cossza}$  must be integrated over the forecast steps to account for variations in solar angles over time.

In this paper, sunlit-average and Gauss–Legendre quadrature integration methodologies were compared. The sunlit-average cosine of the solar zenith

angle, i.e. average over the sunlit share of the timeframe was proven to be efficient (*Hogan and Hirahara, 2016*) and is currently used in the ERA5-HEAT dataset:

$$\overline{\mu_{0m}} = \sin \delta \sin \phi + \frac{\cos \delta \cos \phi (\sin h_{\max} - \sin h_{\min})}{h_{\max} - h_{\min}}, \quad (2)$$

The Gauss–Legendre quadrature method (*Brimicombe, et al., 2022b; Hogan and Hirahara, 2015*) is expressed as:

$$\int_{h_{\min}}^{h_{\max}} f(x) dx \approx \frac{h_{\max} - h_{\min}}{2} \sum_{i=1}^n \omega_i f\left(\frac{h_{\max} - h_{\min}}{2} \xi_i + \frac{h_{\max} + h_{\min}}{2}\right). \quad (3)$$

Here,  $f(x)$  is the instantaneous *cossza*,  $\omega_i$  is weight factor for the numerical integral and  $\xi_i$  is the coordinate of interval boundaries.

In the CERRA system, the direct radiation is represented as the total sky direct shortwave radiation at the surface. To isolate the direct component from the Sun ( $I^*$ ), this total needs to be divided by *cossza*:

$$I^* = \frac{S_{\text{surf}}^{\text{dn,direct}}}{\text{cossza}}, \quad (4)$$

where,  $\text{cossza} > \text{threshold}$  (needs to be defined). Different thresholds were tested for CERRA (0.001, 0.01, 0.03, 0.05, 0.07 and 0.1). These findings have practical implications for MRT computation. For instance, even with the integrated quadrature *cossza*, there's a risk of overestimating MRT when *cossza* approaches 0. This understanding can guide future research and improve the accuracy of MRT calculations in numerical weather prediction models.

Despite using  $S_{\text{surf}}^{\text{dn,direct}}$  directly from CERRA NWP, MRT estimates were also tested using calculated total direct shortwave radiation ( $f_{\text{dir}}$ ) from surface thermal downward radiation, initially written in Fortran and C (*Liljegren et al., 2008*) and rewritten in Cython for Python implementation – PyWBGT library (*Kong and Huber, 2022*) using the exponential ratio:

$$f_{\text{dir}} = \begin{cases} \exp(3 - 1.34 S^* - 1.65/S^*) & \text{for } \text{cossza} = 89.5^\circ, \\ 0 & \text{for } \text{cossza} > 89.5^\circ, \end{cases} \quad (5)$$

where  $S^*$  is the solar irradiance,  $S$ , normalised by the maximum possible solar irradiance outside the atmosphere,  $S_{\max}$  ( $S^* = S/S_{\max}$ ).

The radiation outputs provided by the CERRA NWP system are suitable for calculating MRT, as shown in Eq. (6) (*Di Napoli et al., 2020b*):

$$\text{MRT}^* = \frac{1}{\sigma} \left\{ f_a L_{\text{surf}}^{\text{dn}} + f_a L_{\text{surf}}^{\text{up}} \left[ \frac{a_{\text{ir}}}{\varepsilon_p} + \left( f_a S_{\text{surf}}^{\text{dn,diffuse}} + f_a S_{\text{surf}}^{\text{up}} + f_p I^* \right) \right] \right\}^{0.25}, \quad (6)$$

where:

- $\sigma$  represents the Stefan-Boltzmann constant ( $5.67 \times 10^{-8} \text{W/m}^2\text{K}^4$ );
- $a_{\text{ir}}$  denotes the absorption coefficient of the body surface area irradiated by solar radiation, typically assumed as 0.7;
- $\varepsilon_p$  represents the emissivity of the clothed human body, generally assumed as 0.97;
- $f_a$  is an angle factor set to 0.5, corresponding to the assumption that the surroundings of a human body consist of lower and upper hemispheres (ground and sky), which is valid for macro-scale applications beyond urban settings;
- $f_p$  is the surface projection factor.

### 2.3. Validation against ERA5-HEAT dataset and BSRN station data

MRT derived within the ERA5-HEAT dataset was obtained from C3S CDS (*Di Napoli et al., 2020a*) and based on radiation components from ERA5 (*Hersbach et al., 2018*). The methodology behind the dataset was (*Di Napoli et al., 2020b*) and summarised in a subsequent paper (*Di Napoli et al., 2021*). It was developed with the same spatial ( $0.25^\circ \times 0.25^\circ$ , approx.  $31 \text{ km} \times 31 \text{ km}$ ) and temporal resolution (1 hour) from 1 January 1940 to the present as ERA5.

ERA5-HEAT and CERRA-derived MRT were validated against MRT computed using in-situ measurements of radiation variables from Basile Surface Radiation Network (BSRN) station data (*Driemel et al., 2018*). This network was selected because it can measure radiation variables that are equivalent to those in NWPs. The radiation variables are provided in  $\text{Wm}^{-2}$  for each timestamp. Thus, the instantaneous cossza was applied for MRT computation and then averaged over the forecast step. The 4 available stations for the CERRA domain are available, namely: Cabauw (CAB) in

the Netherlands, Toravere (TOR) in Estonia, Payerne (PAY) in Switzerland and Izaña (IZA) in Tenerife, Spain (Table 1).

Table 1. Elevation of Basile Surface Radiation Network stations compared to ERA5 and CERRA nearest neighbour grid point.

Label	Station	Location	Elevation (m)	ERA5 (m)	CERRA (m)
CAB	Cabauw	The Netherlands	0.0	−0.6	0.6
TOR	Toravere	Estonia	70.0	75.0	74.9
PAY	Payerne	Switzerland	491.0	792.0	480.4
IZA	Izaña	Tenerife, Spain	2372.9	807.0	2290.1

The inter-comparison and validation are based on case studies from one winter and one summer month (January and July 2017). ERA5 data were densified for comparison purposes and resampled on CERRA coordinates using nearest neighbour interpolation. The validation was performed using standard metrics of Taylor diagrams: standard deviation, coefficient of determination, and root mean squared deviation. Additionally, the bias of MRT from NWP against observations was compared. For consistency with previous findings (*Di Napoli et al., 2020b*) and a better alignment between the models and in-situ data, the values were averaged in 3-hour steps. All calculations and analyses were conducted within a Python environment, with significant contributions from the recently published *xclim* and *thermofeel* libraries (*Bourgault et al., 2023; Brimicombe et al., 2022a*).

### 3. Results

#### 3.1. Integration methods of the cosine of the solar zenith angle

Comparing the integration methods of the cosine of the solar zenith angle (*cossza*) shows significant differences in estimates (Fig. 1). Specifically, using the average cosine of the solar zenith angle over the sunlit portion of the timeframe (sunlit-average *cossza*) results in lower integrals for January and higher integrals for July compared to the Gauss-Legendre quadrature integration (quadrature *cossza*) over forecast steps. These differences are consistent across all timestamps and throughout the evaluated *cossza* range. Notably, sunlit-average calculations tend to underestimate MRT dur-

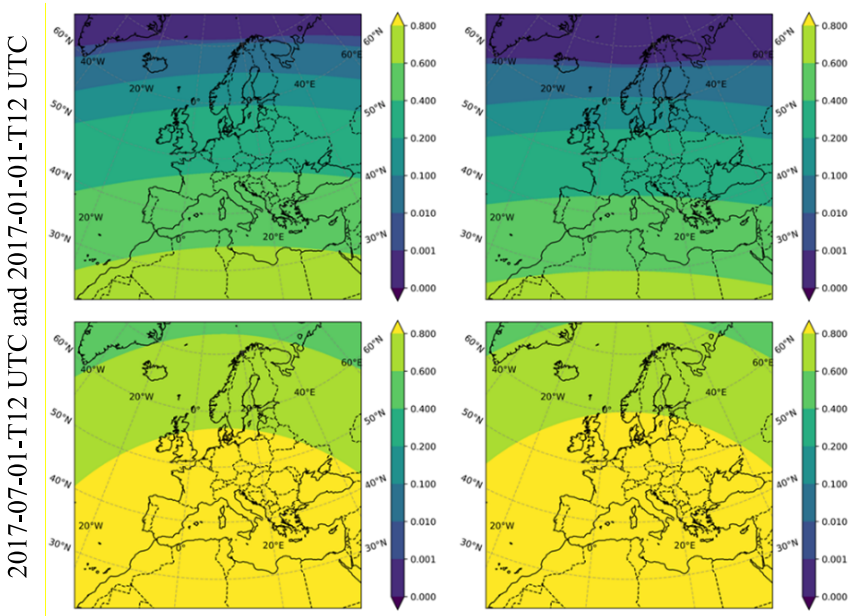


Fig. 1. Quadrature vs sunlit-average cossza.

ing winter months and overestimate it during summer months, with lower discrepancies observed in January and higher differences in July. Particularly during sunrise and sunset hours, the disparities are magnified, which could have an even bigger effect on MRT estimations.

### 3.2. Spatial comparison of CERRA’s vs ERA5-HEAT mean radiant temperature

MRT derived from all implementations of CERRA’s NWP systems generally exhibited lower values compared to those from ERA5-HEAT in January 2017 (Fig. 2). However, there were instances where ERA5 yielded lower MRT than CERRA in specific regions (Figs. 2E,G,I). Across the entire study domain, the MRT differences resulting from various method combinations (including quadrature and sunlit average cossza, as well as using direct components of shortwave radiation from the model and calculated) were found to be comparable to each other. Notably, the MRT differences from the sunlit-average approach did not exceed 0.4 °C (Figs. 2F and H), whereas

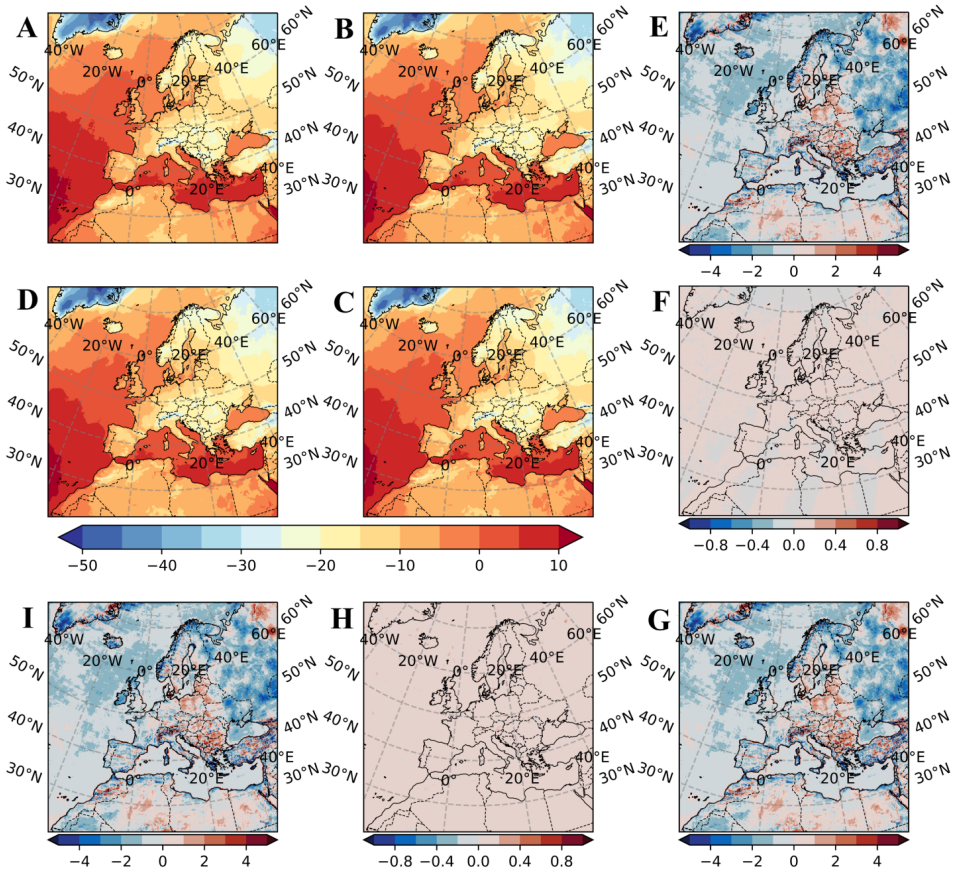


Fig. 2. Mean of daily minimum MRT ( $^{\circ}\text{C}$ ) from A) ERA5-HEAT, B) CERRA quadrature, C) CERRA sunlit-average, D) CERRA sunlit-average with calculated  $f_{\text{dir}}$  and subsequent mean differences (E = B–A, F = C–D, G = C–A, H = C–B, I = D–A, respectively) in January 2017.

those from quadrature cossza and calculated direct radiation ( $f_{\text{dir}}$ ) exhibited slightly larger discrepancies. These patterns persisted consistently throughout the CERRA domain.

Conversely, the MRT derived from CERRA’s NWP systems generally depicted higher values than ERA5-HEAT in July 2017, with differences mostly ranging within 10C. However, there were exceptions, particularly in some areas of northern Africa, where ERA5-HEAT indicated slightly higher

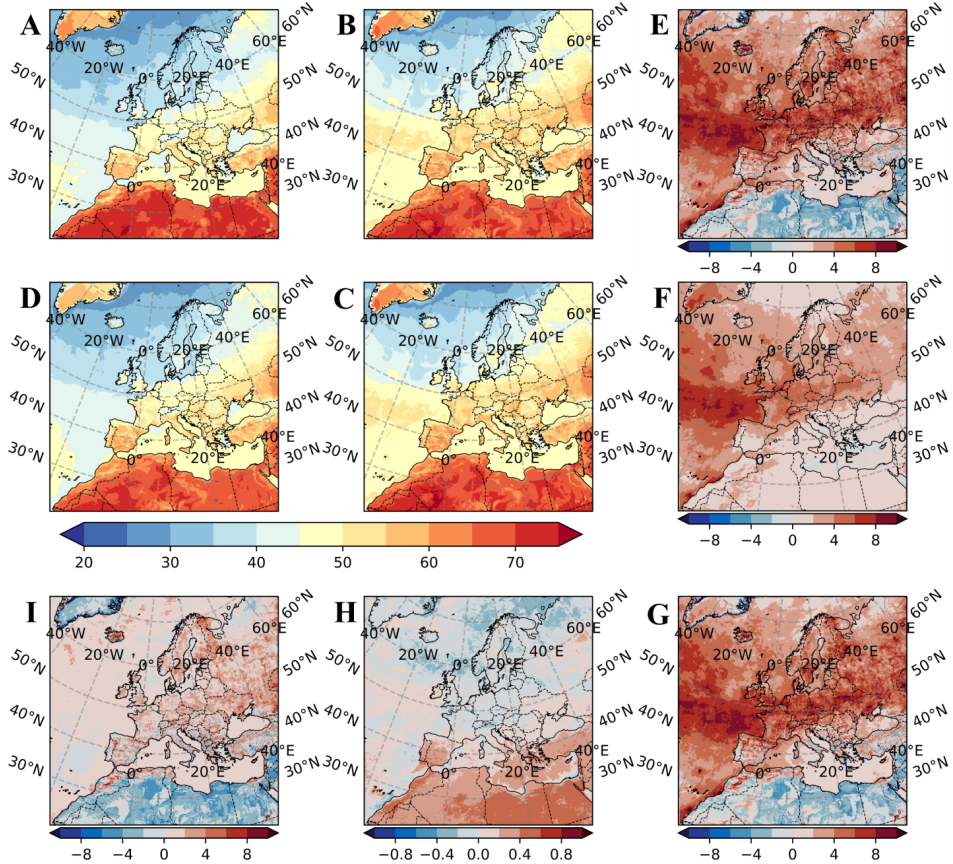


Fig. 3. Mean of daily maximum MRT ( $^{\circ}\text{C}$ ) from A) ERA5-HEAT, B) CERRA quadrature, C) CERRA sunlit-average, D) CERRA sunlit-average with calculated  $f_{\text{dir}}$  and subsequent mean differences (E = B – A, F = C – D, G = C – A, H = C – B, I = D – A, respectively) in July 2017.

MRT than CERRA (Fig. 3). The introduction of the new quadrature cossza method resulted in marginally significant MRT differences ( $< 1^{\circ}\text{C}$ ) compared to January, with higher differences observed in the northern parts and lower differences in the southern regions of the CERRA domain (Fig. 3H). Additionally, when the direct radiation component was calculated, the MRT values were notably lower than those approximated directly from CERRA’s NWP, with differences ranging from 0 to  $6^{\circ}\text{C}$  across various regions (Fig. 3).

### 3.3. Sensitivity of mean radiant temperature to the cosine of the solar zenith angle

The cosine of the solar zenith angle constitutes a pivotal element in the MRT regression function derived from NWP models. As previously mentioned, when the cosine of the solar zenith angle approaches 0, the function tends to yield significant MRT errors, resulting in unexpectedly high values. Therefore, determining an appropriate threshold for dividing  $\text{cossza}$  becomes imperative, where values below the threshold necessitate setting the direct solar radiation component ( $\text{istar}$ ) equal to the total sky direct solar radiation ( $f_{\text{dir}}$ ). In the case of quadrature  $\text{cossza}$ , a threshold of 0.1 may be too large, as evidenced by the pronounced step observed in January, while a threshold of 0.03 already yields visibly elevated MRT values in July. Thus, a threshold of 0.05 emerges as a reasonable compromise, avoiding significant steps in January and preventing higher-than-expected MRT values in July. Conversely, when quadrature  $\text{cossza}$  is utilised in conjunction with calculated  $f_{\text{dir}}$  (rather than direct values from the NWP), a higher threshold of 0.1 may be warranted. For the sunlit-average  $\text{cossza}$  method, the threshold could be set as small as 0.001, effectively mitigating the generation of artificially high MRT values in both January and July 2017.

Direct solar radiation from the CERRA system gives a higher MRT extremes than calculated fluxes (calc.  $f_{\text{dir}}$ ) and ERA5 (Fig. 4).

### 3.4. Validation against observations

The validation process was conducted using data from the Baseline Surface Radiation Network, revealing a strong agreement between the models and station observations. MRT derived from the CERRA models exhibited a performance comparable to ERA5-HEAT in January 2017 (Fig. 5). The coefficient of determination ( $R^2 \approx 0.9$ ) demonstrated consistency across all CERRA methods and ERA5-HEAT, indicating robust agreement. However, when assessed using other metrics such as root mean square error (RMSE) and standard deviation (STD), similar performance was observed for models across stations situated on flat terrain (Cabauw and Toravere). Notably, the CERRA NWP models showcased improved accuracy and reduced uncertainty in MRT estimates for elevated stations, particularly evident at sites like Payerne and Izaña, where the RMSE decreased from 10 for ERA5-HEAT to less than 5 for CERRA models.

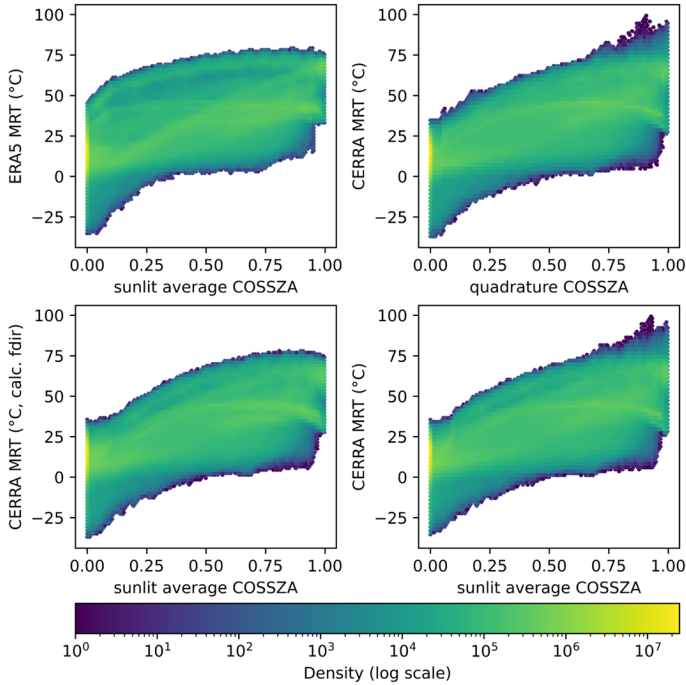


Fig. 4. Sensitivity of mean radiant temperature from cosine of solar zenith angle in July 2017. ERA5 MRT interpolated on CERRA coordinates to obtain the same density of data values.

MRT estimates from CERRA models surpassed those from ERA5-HEAT across all stations in July 2017 (Fig. 6). This superiority was consistently demonstrated across all metrics, including standard deviation, root mean square error, and coefficient of determination, indicative of enhanced precision, accuracy, and reduced uncertainty attributable to CERRA NWP. Similarly, minimal disparities were observed between the quadrature and sunlit-average cossza integration methods. When the  $f_{dir}$  is calculated, the loss of quality is visible and could be important for MRT extremes.

### 3.5. Bias of mean radiant temperature

The bias between MRT derived from NWP and observations was assessed. For stations situated on flat terrain, such as Cabauw and Toraverre, both ERA5-HEAT and CERRA exhibited comparable mean biases,

with both NWP models slightly underestimating MRT. Notably, ERA5-HEAT showed a slight advantage over CERRA, particularly evident at Toravere station, where the former model exhibited approximately 1 °C lower bias. Conversely, the CERRA system demonstrated a significant improvement in MRT precision compared to ERA5-HEAT for stations located at higher elevations, with biases averaging around 0 °C. Notably, ERA5-HEAT exhibited underestimation for the Payerne station in Switzerland (approximately −3 °C) and overestimation for the Izaña station in Tenerife, Spain (approximately +3 °C).

The results depicted in Fig. 7 illustrate the mean bias of MRT from NWP models against observations for July 2017. Similar precision outcomes were observed for the winter period, albeit with notable differences. Specifically, in winter, ERA5-HEAT showed even higher overestimation for the Izaña station (approximately +9 °C, not shown). Unexpectedly, the CERRA sys-

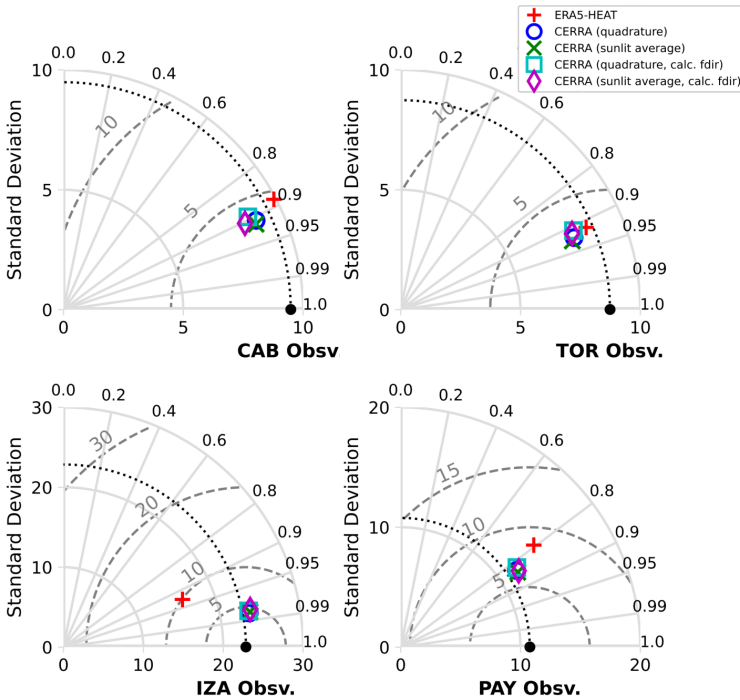


Fig. 5. Validation against observations in January 2017 (Taylor diagrams:  $R^2$  as radial axis, STD as angular axis, centred RMSE contours in dashed grey).

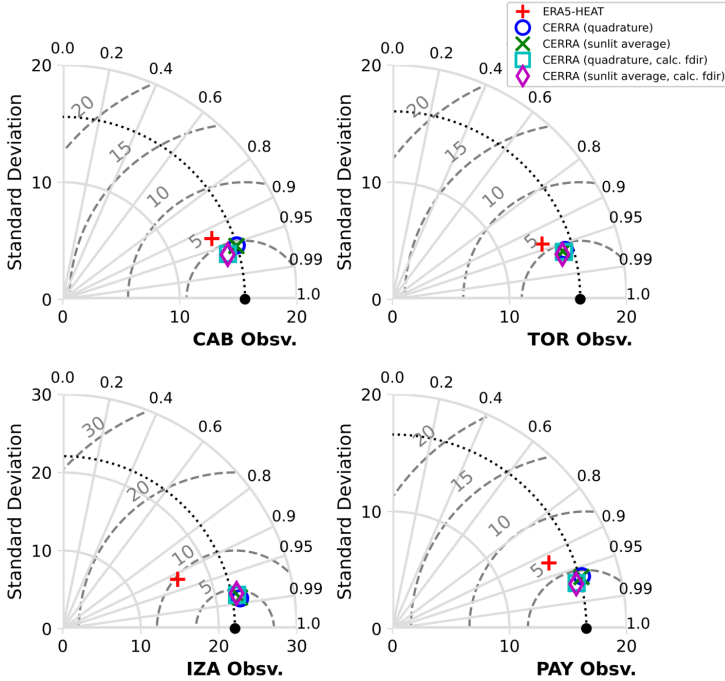


Fig. 6. Validation against observations in July 2017 (Taylor diagrams:  $R^2$  as radial axis, STD as angular axis, centred RMSE contours in dashed grey).

tem showcased improved MRT precision for stations located at higher elevations compared to those on plain terrain, defying conventional expectations. Moreover, no significant discrepancy was observed between the quadrature and sunlit-average cossza integration methods. However, it is worth noting that calculated total sky direct solar radiation exhibited slightly worse precision compared to the values obtained directly from the CERRA system output. In conclusion, the CERRA system’s enhanced spatial resolution offers a significant improvement in MRT estimation, particularly benefiting elevated and coastal areas.

#### 4. Discussion and conclusions

Different methods of integrating the cosine of the solar zenith angle (cossza) show observed differences in estimations of MRT. Using the sunlit-average cossza tends to be underestimated in winter and overestimated in summer,

with magnified discrepancies during sunrise and sunset hours. However, those disparities showed a neglected effect on mean radiant temperature (MRT). These results are in line with previous findings (*Brimicombe et al., 2023; Brimicombe et al., 2022b; Hogan and Hirahara, 2015*). Sunlit-average cossza may be more applicable for climate services and quadrature for forecasting integration.

This is not the case when the direct solar downward radiation is used directly from the CERRA system (*Schimanke et al., 2021*) and calculated using the exponential ratio (*Liljegren et al., 2008*). The overall differences ( $< 1^{\circ}\text{C}$ ) are not that substantial (as evidenced by Figs. 5–7), while this has significant importance for MRT daily maximums (even  $6^{\circ}\text{C}$  for the land area) and extremes in summer (Figs. 3 and 4, respectively). However,

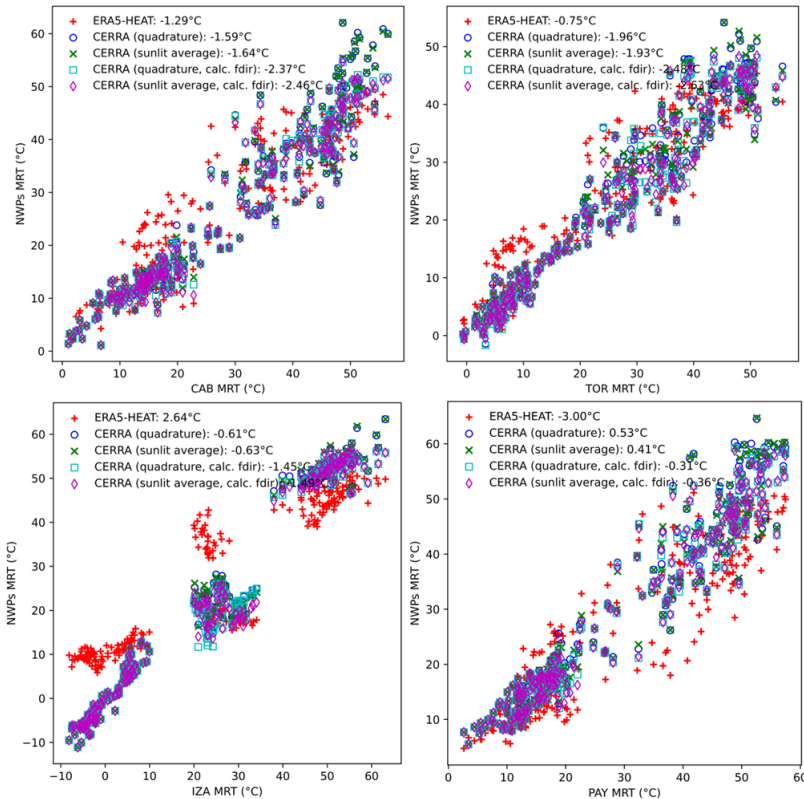


Fig. 7. Mean bias of MRT from NWPs against observations with values in July 2017.

the calculated version could be used when direct radiation is not available, specifically for future shared socio-economic pathways and representative concentration pathways (CMIP6 climate projections). It could be compared with numerical methods for future thermal stress quantifications.

The MRT values are sensitive to the cosine of the solar zenith angle when it's close to 0. Determining an appropriate threshold for dividing  $\cos\theta$  is imperative to avoid significant errors in MRT estimates. Including downwelling direct shortwave radiation to the CERRA variables outputs could be very beneficial for quantifying thermal comfort and stress indices. Especially if elevation and topography could be considered in solar declination angle for  $\cos\theta$  calculations.

Daily minimum MRT derived from CERRA NWP systems was comparable to ERA5-HEAT in winter. CERRA generally depicted higher values in summer than ERA5-HEAT, with differences mostly within 10 °C. However, exceptions were observed in some areas of northern Africa.

Validation against observations showed strong agreement between the models and station observations. CERRA models performed comparably to ERA5-HEAT in January and July 2017 for stations on flat terrain. Meanwhile, CERRA demonstrated reduced uncertainty and improved accuracy and precision for elevated stations.

It is worth acknowledging that our study is focused on January and July 2017, and the model's performance could vary in other years or under different meteorological conditions. Additionally, ERA5-HEAT has a much larger resolution compared to CERRA (approx. 31 km and 5.5 km, respectively). The results are reasonable for plains and plateaus, although this has implications for elevated and coastal locations where the radiation budget has been changed.

The CERRA system's enhanced spatial resolution significantly improves MRT quantification, especially in elevated and coastal areas. Beyond MRT estimation and forecasting, potential applications include human biometeorological indices (PET, WBGT, UTCI), public health assessments, and serving as a proxy for microclimate modelling in urban areas (e.g., ENVI-met and SOLWEIG). Future research could explore comparisons with numerical methods for thermal stress quantification and further investigate the system's performance in diverse geographical settings. Additionally, efforts to improve direct solar radiation data integration into NWP systems

could enhance the accuracy of temperature estimation and provide valuable insights into climate change impacts on thermal comfort and health.

- High-resolution CERRA data (5.5 km) significantly improves MRT estimation accuracy, particularly in complex terrains (mountains, coasts), compared to the coarser ERA5-HEAT dataset across Europe.
- While different cossza integration methods yield similar overall MRT results, the calculation or use of direct solar radiation notably affects summer maximum MRT values.
- This validated approach provides more reliable MRT inputs for thermal stress assessments, especially in regions poorly represented by lower-resolution models.

**Acknowledgements.** O. Skrynyk gratefully acknowledges the Earth Science Institute of the Slovak Academy of Sciences for its hospitality and the SAIA's National Scholarship Programme of the Slovak Republic for its support. This research builds upon a project supported by the National Science Centre, Poland (ref. no. 2020/37/N/ST10/03090).

## References

- Bazile E., Abida R., Verelle A., Le Moigne P., Szczypta C., 2017: MESCAN-SURFEX surface analysis, deliverable D2.8 of the UERRA project, <http://www.uerra.eu/publications/deliverable-reports.html>.
- Bażejczyk K., Kunert A., 2011: Bioklimatyczne uwarunkowania rekreacji i turystyki w Polsce (Bioclimatic principles of recreation and tourism in Poland). IGiPZ PAN, Warszawa (in Polish).
- Bourgault P., Huard D., Smith T. J., Logan T., Aoun A., Lavoie J., Dupuis É., Rondeau-Genesse G., Alegre R., Barnes C., Laperrière A. B., Biner S., Caron D., Ehbrecht C., Fyke J., Keel T., Labonté M.-P., Lierhammer L., Low J.-F., Quinn J., Roy P., Squire D., Stephens A., Tanguy M., Whelan C., 2023: xclim: xarray-based climate data analytics. *J. Open Source Softw.*, **8**, 85, 5415, doi: 10.21105/joss.05415.
- Brimicombe C., Di Napoli C., Quintino T., Pappenberger F., Cornforth R., Cloke H. L., 2022a: Thermofeel: A python thermal comfort indices library. *SoftwareX*, **18**, 101005, doi: 10.1016/j.softx.2022.101005.
- Brimicombe C., Lo C. H. B., Pappenberger F., Di Napoli C., Maciel P., Quintino T., Cornforth R., Cloke H. L., 2023: Wet bulb globe temperature: Indicating extreme heat risk on a global grid. *GeoHealth*, **7**, 2, e2022GH000701, doi: 10.1029/2022GH000701.
- Brimicombe C., Quintino T., Smart S., Di Napoli C., Hogan R. J., Cloke H. L., Pappenberger F., 2022b: Calculating the cosine of the solar zenith angle for thermal comfort indices. ECMWF Technical Memorandum, 895, doi: 10.21957/o7pcu1x2b.

- Di Napoli C., Barnard C., Prudhomme C., Cloke H. L., Pappenberger F., 2020a: Thermal comfort indices derived from ERA5 reanalysis [Dataset]. Copernicus Climate Change Service (C3S) Climate Data Store (CDS), doi: 10.24381/cds.553b7518.
- Di Napoli C., Barnard C., Prudhomme C., Cloke H. L., Pappenberger F., 2021: ERA5-HEAT: A global gridded historical dataset of human thermal comfort indices from climate reanalysis. *Geosci. Data J.*, **8**, 1, 2–10, doi: 10.1002/GDJ3.102.
- Di Napoli C., Hogan R. J., Pappenberger F., 2020b: Mean radiant temperature from global-scale numerical weather prediction models. *Int. J. Biometeorol.*, **64**, 7, 1233–1245, doi: 10.1007/s00484-020-01900-5.
- Driemel A., Augustine J., Behrens K., Colle S., Cox C., Cuevas-Agulló E., Denn F. M., Duprat T., Fukuda M., Grobe H., Haefelin M., Hodges G., Hyett N., Ijima O., Kallis A., Knap W., Kustov V., Long C. N., Longenecker D., Lupi A., Maturilli M., Mimouni M., Ntsangwane L., Ogihara H., Olano X., Olefs M., Omori M., Passamani L., Pereira E. B., Schmithüsen H., Schumacher S., Sieger R., Tamlyn J., Vogt R., Vuilleumier L., Xia X., Ohmura A., König-Langlo G., 2018: Baseline Surface Radiation Network (BSRN): Structure and data description (1992–2017). *Earth Syst. Sci. Data*, **10**, 3, 1491–1501, doi: 10.5194/essd-10-1491-2018.
- Gál C. V., Kántor N., 2020: Modeling mean radiant temperature in outdoor spaces, A comparative numerical simulation and validation study. *Urban Clim.*, **32**, 100571, doi: 10.1016/j.uclim.2019.100571.
- Hersbach H., Bell B., Berrisford P., Biavati G., Horányi A., Muñoz-Sabater J., Nicolas J., Peubey C., Radu R., Rozum I., Schepers D., Simmons A., Soci C., Dee D., Thépaut J.-N., 2018: ERA5 hourly data on single levels from 1940 to present [Dataset]. Copernicus Climate Change Service (C3S) Climate Data Store (CDS), doi: 10.24381/cds.adbb2d47.
- Hersbach H., Bell B., Berrisford P., Hirahara S., Horányi A., Muñoz-Sabater J., Nicolas J., Peubey C., Radu R., Schepers D., Simmons A., Soci C., Abdalla S., Abellan X., Balsamo G., Bechtold P., Biavati G., Bidlot J., Bonavita M., De Chiara G., Dahlgren P., Dee D., Diamantakis M., Dragani R., Flemming J., Forbes R., Fuentes M., Geer A., Haimberger L., Healy S., Hogan R. J., Hólm E., Janisková M., Keeley S., Laloyaux P., Lopez P., Lupu C., Radnoti G., de Rosnay P., Rozum I., Vamborg F., Villaume S., Thépaut, J.-N., 2020: The ERA5 global reanalysis. *Q. J. R. Meteorol. Soc.*, **146**, 730, 1999–2049, doi: 10.1002/qj.3803.
- Hogan R. J., 2015: Radiation Quantities in the ECMWF model and MARS. ECMWF report. Available at <https://www.ecmwf.int/en/eLibrary/80755-radiation-quantities-ecmwf-model-and-mars>.
- Hogan R. J., Hirahara S., 2015: Effect of solar zenith angle specification on mean shortwave fluxes and stratospheric temperatures. ECMWF Technical Memorandum, 758, doi: 10.21957/jwv20er1v.
- Hogan R. J., Hirahara S., 2016: Effect of solar zenith angle specification in models on mean shortwave fluxes and stratospheric temperatures. *Geophys. Res. Lett.*, **43**, 1, 482–488, doi: 10.1002/2015GL066868.
- Höppe P., 1999: The physiological equivalent temperature – a universal index for the biometeorological assessment of the thermal environment. *Int. J. Biometeorol.*, **43**, 2,

- 71–75, doi: 10.1007/s004840050118.
- ISO 7726:1998, 1998: Ergonomics of the thermal environment—Instruments for measuring physical quantities. ISO, <https://www.iso.org/standard/14562.html>.
- Kong Q., Huber M., 2022: Explicit calculations of wet-bulb globe temperature compared with approximations and why it matters for labor productivity. *Earth's Future*, **10**, 3, e2021EF002334, doi: 10.1029/2021EF002334.
- Krüger E. L. (Ed.), 2021: Applications of the Universal Thermal Climate Index UTCI in biometeorology: latest developments and case studies. Springer International Publishing, doi: 10.1007/978-3-030-76716-7.
- Liljegren J. C., Carhart R. A., Lawday P., Tschopp S., Sharp R., 2008: Modeling the wet bulb globe temperature using standard meteorological measurements. *J. Occup. Environ. Hyg.*, **5**, 10, 645–655, doi: 10.1080/15459620802310770.
- Lindner-Cendrowska K., Baranowski J., 2023: Niepewność pomiarów średniej temperatury promieniowania za pomocą termometrów kulistych (Uncertainty of mean radiant-temperature measurements using globe thermometers). *Przegląd Geograficzny*, **95**, 3, 271–290, doi: 10.7163/PrzG.2023.3.4 (in Polish with English abstract).
- McGregor G. R., 2012: Special issue: Universal Thermal Comfort Index (UTCI). *Int. J. Biometeorol.*, **56**, 3, 419–419, doi: 10.1007/S00484-012-0546-6.
- Ridal M., Bazile E., Le Moigne P., Randriamampianina R., Schimanke S., Andrae U., Berggren L., Brousseau P., Dahlgren P., Edvinsson L., El-Said A., Glinton M., Hagelin S., Hopsch S., Isaksson L., Medeiros P., Olsson E., Unden P., Wang Z. Q., 2024: CERRA, the Copernicus European Regional Reanalysis system. *Q. J. R. Meteorol. Soc.*, **150**, 763, 3385–3411, doi: 10.1002/qj.4764.
- Schimanke S., Ridal M., Le Moigne P., Berggren L., Undén P., Randriamampianina R., Andrea U., Bazile E., Bertelsen A., Brousseau P., Dahlgren P., Edvinsson L., El Said A., Glinton M., Hopsch S., Isaksson L., Mladek R., Olsson E., Verrelle A., Wang Z. Q., 2021: CERRA sub-daily regional reanalysis data for Europe on single levels from 1984 to present [Dataset]. Copernicus Climate Change Service (C3S) Climate Data Store (CDS), doi: 10.24381/cds.622a565a.
- Soci C., Bazile E., Besson F., Landelius T., 2016: High-resolution precipitation re-analysis system for climatological purposes. *Tellus A, Dynamic Meteorology and Oceanography*, **68**, 1, 29879, doi: 10.3402/tellusa.v68.29879.
- Thorsson S., Lindberg F., Eliasson I., Holmer B., 2007: Different methods for estimating the mean radiant temperature in an outdoor urban setting. *Int. J. Climatol.*, **27**, 14, 1983–1993, doi: 10.1002/joc.1537.
- Vanos J. K., Rykaczewski K., Middel A., Vecellio D. J., Brown R. D., Gillespie T. J., 2021: Improved methods for estimating mean radiant temperature in hot and sunny outdoor settings. *Int. J. Biometeorol.*, **65**, 6, 967–983, doi: 10.1007/s00484-021-02131-y.
- VDI, 2008: VDI 3787-2, Environmental Meteorology—Methods for the Human Biometeorological Evaluation of Climate and Air Quality for Urban and Regional Planning at Regional Level. Part 1: Climate. Beuth, Berlin.
- Voogt J. A., Oke T. R., 2003: Thermal remote sensing of urban climates. *Remote Sens. Environ.*, **86**, 3, 370–384, doi: 10.1016/S0034-4257(03)00079-8.

- Wang C., Zhan W., Liu Z., Li J., Li L., Fu P., Huang F., Lai J., Chen J., Hong F., Jiang, S., 2020: Satellite-based mapping of the Universal Thermal Climate Index over the Yangtze River Delta urban agglomeration. *J. Clean. Prod.*, **277**, 123830, doi: 10.1016/j.jclepro.2020.123830.